Available online at www.sciencedirect.com
ScienceDirect
Catalysis Today 133–135 (2008) 344–350
CATALYSIS TODAY
www.elsevier.com/locate/cattod

# Hydrogen production in membrane reactors using Rh catalysts on binary supports

Carlos Carrara [a], Alejandro Roa [a], Laura Cornaglia [a,*], Eduardo A. Lombardo [a], Cecilia Mateos-Pedrero [b], Patricio Ruiz [b]

[a] *Instituto de Investigaciones en Catálisis y Petroquímica (FIQ, UNL-CONICET), Sgo del Estero 2829-3000 Santa Fe, Argentina*
[b] *Unité de Catalyse et Chimie des Matériaux Divisés, Université Catholique de Louvain, Place Croix du Sud 2/17, 1348 Louvain-la Neuve, Belgium*

Available online 24 January 2008

**Abstract**

The binary supports employed in this work were prepared by different methods. The Ti(7%)–MgO and the Ti(13%)–$SiO_2$ were obtained using the grafting technique. The La(27%)–$SiO_2$ was obtained through the incipient wetness impregnation with $La(NO_3)_3$ of Aerosil 300, previously calcined at 1173 K. The Rh was incorporated to these supports by wet impregnation. The catalysts were first evaluated for the $CH_4 + CO_2$ reaction in a fixed-bed reactor. They were found to be active and stable as to justify their use in the membrane reactor, which was operated at 823 K achieving methane conversions up to twice as much as the equilibrium values. In all cases, the activity of the Rh solids remained constant after 120 h on stream with very little formation of carbonaceous residues only detected through LRS. The catalysts were characterized through either hydrogen or carbon monoxide chemisorption, TPR, XRD, LRS and XPS. The Rh(0.6)/La–$SiO_2$ catalyst showed a high metal dispersion that remained constant after use and the highest capacity to restore the $CH_4 + CO_2$ equilibrium when $H_2$ was permeated out of the reaction section. The Rh(0.8)/Ti–MgO showed the highest Rh/oxide interaction associated with the lowest capacity to restore the reaction equilibrium. The Rh(0.8)/Ti–$SiO_2$ exhibited an intermediate activity due in part to the partial segregation of the $TiO_2$ upon calcinations and the subsequent appearance of small $Rh^\circ$ crystallites in the used catalysts.


*Keywords:* Dry reforming; Methane; Ti–MgO; Ti–$SiO_2$; La–$SiO_2$

## 1. Introduction

In previous papers, it was shown that Rh-containing catalysts can be used to obtain ultrapure hydrogen through the $CH_4 + CO_2$ reaction using membrane reactors [1,2]. For this application the catalyst should be active and stable at ca. 823 K with no carbon formation. In the case of Rh/$La_2O_3$ the stability of this active catalyst is due to the strong interaction between the metal and the oxide. Besides, the very low amount of carbon deposited on this catalyst is due to the presence of oxycarbonates that remove most of the carbon formed from methane decomposition [1,3].

The use of mixed supports for this type of catalysts is very attractive in view of the good results obtained for the partial oxidation of methane with $TiO_2$–MgO and $TiO_2$–$SiO_2$ [4]. In the same vein, Vidal et al. [5] reported values of up to 100% dispersion for Rh supported on $La_2O_3$–$SiO_2$.

Different types of materials have been used in membrane reactors to obtain hydrogen, among them silica modified alumina [6] and thin palladium films [7]. In previous studies, we reported [1,2] that both hydrogen production and methane conversion could be greatly improved by removing the $H_2$ formed using a stable and 100% selective Pd–Ag dense 50 μm thick membrane.

In this work, Ti–MgO, Ti–$SiO_2$ and La–$SiO_2$ were used as Rh supports. In the first two cases the surfaces of both oxides were modified by grafting Ti on them. In the latter case, the lanthanum salt was impregnated on the oxide. Hydrogen and CO chemisorption, TPR, XRD, LRS and XPS were used to

* Corresponding author.
*E-mail address:* lmcornag@fiqus.unl.edu.ar (L. Cornaglia).

0920-5861/$ – see front matter © 2007 Elsevier B.V. All rights reserved.
doi:10.1016/j.cattod.2007.12.016

characterize the supports and the catalysts, fresh and after use, in the dry reforming of methane.

## 2. Experimental

### 2.1. Catalyst preparation

The binary supports employed in this work were prepared by different methods. The Ti–MgO and the Ti–$SiO_2$ supports were obtained using the grafting technique. Prior to grafting, the oxides (MgO and $SiO_2$) were dried at 393 K during 16 h. The titanium was deposited on MgO with a solution of $TiCl_4$ (Acros Organics, pure grade) in hexane (Merk, 99+%). The incorporation of titanium onto $SiO_2$ was performed with Ti $[OCH(CH_3)_2]_4$ (Aldrich, pure grade) in isopropanol (Aldrich 99+%). In both solids, the titania amount corresponds to the theoretical monolayer (13 and 7 wt.% $TiO_2$, for Ti–$SiO_2$ and Ti–MgO solids, respectively) and was calculated as described elsewhere [4]. The Rh/Ti–MgO and Rh/Ti–$SiO_2$ catalysts (0.8 wt.% Rh) were obtained by wet impregnation of supports with an aqueous solution of $(NH_4)_3RhCl_6{\cdot}3H_2O$ (Aldrich, 28 wt.% Rh). The catalysts were dried overnight at 383 K and then calcined in flowing air at 973 K during 4 h.

The La–$SiO_2$ support was obtained through the incipient wetness impregnation of $SiO_2$ (Aerosil 300), previously calcined at 1173 K with $La(NO_3)_3$ (Anedra). The $La_2O_3$ amount (27 wt.%) also corresponded to the theoretical monolayer. The solid was calcined at 873 K; the metal deposition was performed with $RhCl_3{\cdot}3H_2O$ (Alfa) as precursor compound; and the Rh/La–$SiO_2$ was obtained by incipient wetness impregnation of La–$SiO_2$ with 0.6 wt.% Rh. The sample was kept at room temperature for 4 h, dried at 343 K overnight and then calcined in flowing air at 823 K during 6 h.

### 2.2. Catalyst characterization

#### 2.2.1. BET measurements

The BET surface area was determined from $N_2$ adsorption at liquid nitrogen temperature using a Micromeritics TriStar 3000 instrument. Surface areas were calculated by the BET method. Prior to measurements, all samples were degassed at 423 K under a 0.13 Pa overnight

#### 2.2.2. X-ray diffraction (XRD)

The XRD patterns of the solids were obtained with an XD-D1 Shimadzu instrument, using Cu Kα radiation at 35 kV and 40 mA. The scan rate was 1 °/min in the range $2\theta = 10–80°$.

#### 2.2.3. Temperature-programmed reduction (TPR)

An Okura TP-20022S instrument equipped with TCD was used for the TPR experiments. To eliminate the carbonates present in the Rh/La–$SiO_2$ samples, the following pretreatment was used: the solid was heated up to 823 K in oxygen flow, kept constant for half an hour and then cooled down in Ar flow. Afterwards, it was reduced in a 5% $H_2$–Ar stream, with a heating rate of 10 K/min up to the maximum treatment temperature. In the case of the Rh/$SiO_2$, Rh/Ti–MgO and the Rh/Ti–$SiO_2$ samples, TPR experiments were conducted by heating the sample from room temperature to 973 K under the same reduction conditions.

#### 2.2.4. Metal dispersion

The Rh dispersion of the Rh/La–$SiO_2$ catalysts was determined by static equilibrium of CO adsorption at room temperature in a conventional vacuum system. The CO uptakes were calculated taking into account the three adsorption states (linear, bridge and gem). The contribution of each one was evaluated by a fit of the FTIR bands using Lorentzian functions. The integral extinction coefficients and stoichiometric factors were taken from Knozinger and co-workers [8]. With the same experimental setup but using $H_2$, the metal dispersion of Rh/$SiO_2$ was calculated. In the case of the Rh/Ti–MgO and the Rh/Ti–$SiO_2$ catalysts, the dispersion of Rh was determined by $H_2$ chemisorption on a static volumetric apparatus Micromeritics ASAP2010 C adsorption analyzer. The catalysts were first reduced at 873 K under a pure $H_2$ flow during 1 h, then flushed under He at 923 K during 2 h and cooled down under He to room temperature. After evacuation of the sample the chemisorption was performed at room temperature. A first isotherm was recorded to evaluate the volumes of physisorbed and chemisorbed gas. A second isotherm was used to determine the fraction reversibly adsorbed. The difference between both isotherms provided the chemisorbed volume of $H_2$. In all cases the H/Rh° stoichiometry was assumed to be 1/1.

#### 2.2.5. XPS analyses

All the samples were analyzed with an Axis Ultra spectrometer from Kratos working with a non-monochromatic Mg radiation (10 kV, 15 mA) and the charge compensation device provided by the supplier (charge balance fixed at −2.3 V). The sample powders were pressed into small stainless steel troughs mounted on a multi-specimen holder. The pressure in the analysis chamber was around $10^{-6}$ Pa. The angle between the normal to the sample surface and the lens axis was 0°. The hybrid lens magnification mode was used with the slot aperture resulting in an analyzed area of 700 μm × 300 μm. The pass energy for the analyzer was 40 eV. In these conditions, the energy resolution gives a full width at half maximum (FWHM) of the Ag $3d_{5/2}$ peak of about 1 eV. The following sequence of spectra was recorded: survey spectrum, C 1s, O 1s, Mg 2s, Ti 2p, La 3d, Si 2p, Rh 3d, and C 1s again to check the stability of the charge compensation as a function of time and the absence of degradation of the sample during the analyses. The binding energies were calibrated by fixing the C–(C, H) contribution of the C 1s adventitious carbon at 284.8 eV. Peaks were considered to be combinations of Gaussian and Lorentzian functions in a 70/30 ratio working with linear baseline. For the quantification of the elements, sensitivity factors provided by the manufacturers were used. Data treatment was performed with the Casa XPS program (Casa Software Ltd., UK).

#### 2.2.6. Thermogravimetric analysis (TGA)

The presence of carbon on the used catalysts was investigated by oxidizing the carbon in a Mettler Toledo

TGA/SDTA (Model 851) system. The used catalysts (usually 10 mg) were heated at 10 K/min to 1173 K in a flow of 90 ml/min air.

#### 2.2.7. Laser Raman spectroscopy (LRS)

The Raman spectra were recorded with a TRS-600-SZ-P Jasco Laser Raman instrument, equipped with a charge-coupled device (CCD) with the detector cooled to about 153 K using liquid $N_2$. The excitation source was the 514.5 nm line of a Spectra 9000 Photometrics Ar ion laser. The laser power was set at 30 MW.

### 2.3. Catalytic tests

#### 2.3.1. Fixed-bed reactor

The catalyst (50 mg, dp $<$ 150 μm) was loaded into a tubular quartz reactor (inner diameter, 5 mm), which was placed in an electric oven. A thermocouple in a quartz sleeve was placed on top of the catalyst bed. The catalysts were heated in flowing He at 973 K and then reduced in situ in pure $H_2$ at 823 K for 3 h. After reduction, the reactor was flushed with He and the feed gas mixture (33% $CH_4$, v/v, 33% $CO_2$, 34% He, $P = 1$ atm) was switched to the reactor. The stability tests were carried out at $W/F = 4.4 \times 10^{-6}$ g h ml$^{-1}$. The reaction products were analyzed in a TCD gas chromatograph (Shimadzu GC-8A) equipped with a Porapak and a molecular sieve column.

#### 2.3.2. Membrane reactor

The double tubular membrane reactor was built using a commercial dense Pd–Ag alloy (inner tube), provided by REB Research and Consulting, with one end closed and an inner tube to allow helium sweep gas flow. The outer tube was made of commercial non-porous quartz (i.d. 9 mm). The catalyst, diluted with quartz chips to obtain the 8 cm bed height, was packed in the outer annular region (shell side). The permeation area was $8.0 \times 10^{-4}$ m$^2$. The inner side of the membrane in all runs was kept at atmospheric pressure. More details were previously reported [1]. The catalysts were heated in He at 823 K and then reduced in situ in flowing pure $H_2$ at the same temperature for 3 h. After reduction, the feed stream gas mixture (33% $CH_4$, v/v, 33% $CO_2$, 34% He, $P = 1$ atm) was switched through the reactor. In order to measure the equilibrium conversions, the membrane reactor was operated with neither sweep gas nor pressure difference between the tube and the shell sides. The conversions were measured after a 12 h stabilization period.

## 3. Results

### 3.1. Catalytic behavior

#### 3.1.1. Fixed-bed reactor

Table 1 shows the reaction rates measured with the three catalysts. Note the high Rh exposure in the La–$SiO_2$ solid. The highest reaction rates are observed for the Rh/Ti–$SiO_2$ system. Fig. 1 shows that the catalysts assayed maintain their activity beyond 100 h on stream.

Table 1
Catalytic activity measured at 823 K in the fixed-bed reactor[a]

| Catalyst[b] | $D$ (%) | $r_{CH_4}$ (mol h$^{-1}$ g cat$^{-1}$) | $r_{CO_2}$ (mol h$^{-1}$ g cat$^{-1}$) | $S_{BET}$ (m$^2$ g$^{-1}$) |
|---|---|---|---|---|
| Rh(0.8)Ti–MgO | 14[c] | 0.27 | 0.41 | 52 |
| Rh(0.8)Ti–$SiO_2$ | 15[c] | 0.42 | 0.58 | 97 |
| Rh(0.6)La–$SiO_2$ | 79[d] | 0.30 | 0.51 | 150 |

[a] Conditions: 33% $CH_4$, 33% $CO_2$, 34% Ar, $T$ 823 K, $P = 1$ atm.
[b] Reduced at 823 K for 3 h.
[c] Measured by $H_2$ chemisorption.
[d] Measured by CO chemisorption.

#### 3.1.2. Membrane reactor

The difference in hydrogen partial pressure is the driving force for its permeation. By increasing the sweep gas flow, the partial pressure of hydrogen decreases and favors its permeation through the membrane. Fig. 2 shows the effect of the sweep gas flow rate upon hydrogen production. Beyond 70 ml min$^{-1}$ a plateau was reached. This means that above this flow rate, only a marginal increase of hydrogen production is observed.

To further characterize the catalytic differences among the catalysts, a variable $\eta$ is defined that measures the deviation from equilibrium for the reaction ($CH_4 + CO_2 \leftrightarrow 2CO + 2H_2$), $\eta = \Pi p_i^{\upsilon i}/K_{eq}$. In this equation, $p_i$ is the measured partial pressure of each component, $\upsilon i$ the stoichiometric coefficients

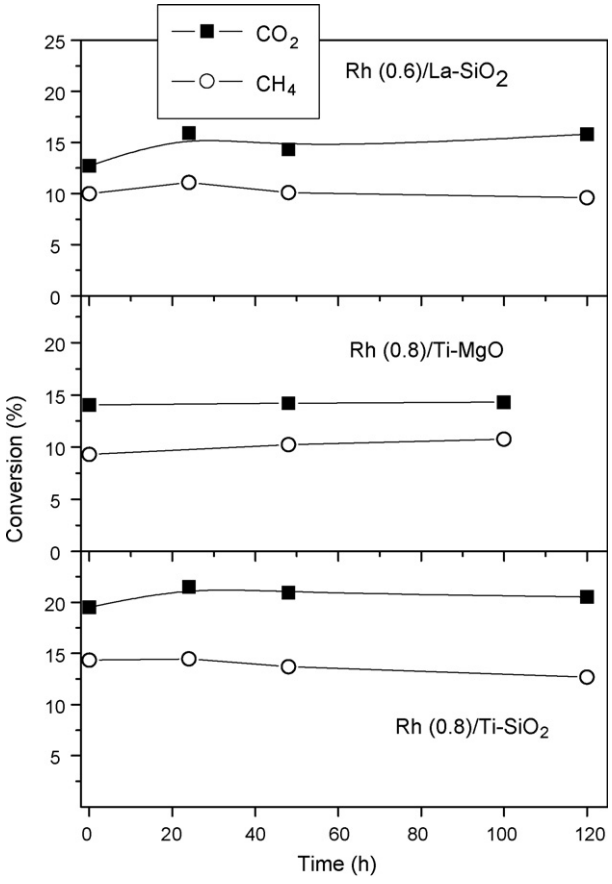


Fig. 1. Stability test of the catalysts in the fixed-bed reactor. Conditions: feed gas composition 33% $CH_4$, 33% $CO_2$, 34% Ar, $T$ 823 K, $P = 1$ atm, $W/F = 4.4 \times 10^{-6}$ g h ml$^{-1}$.

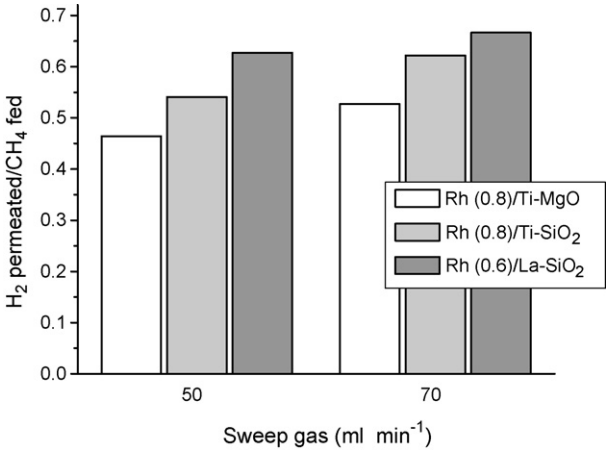


Fig. 2. Effect of sweep gas flow rate upon hydrogen production. Conditions: same as in Fig. 1, $W/F = 1 \times 10^{-3}$ g h ml$^{-1}$.

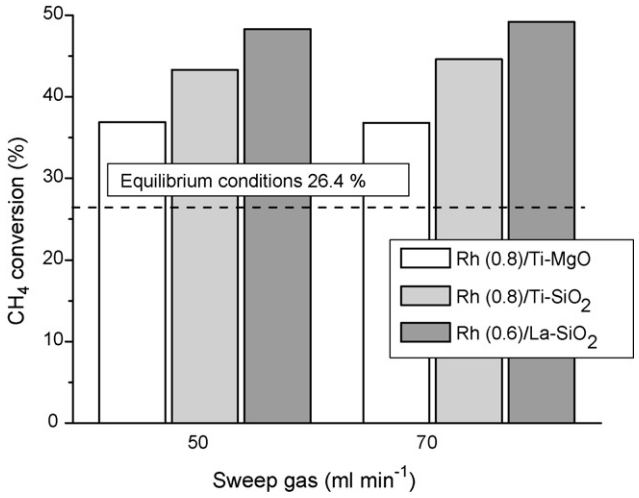


Fig. 4. Differences in the membrane reactor performance of the three catalysts. Conditions: same as in Fig. 2.

of reactants and products, and $K_{eq}$ is the experimental equilibrium constant evaluated in the membrane reactor operating as fixed-bed. $\eta = 1$ when the system is at equilibrium.

Fig. 3 shows how the system deviates from equilibrium as the sweep gas flow rates increase. This plot evaluates the ability of the catalysts to restore the equilibrium when hydrogen is withdrawn from the reacting zone. Note that this ratio decreases more slowly when the Rh/La–$SiO_2$ catalyst is used. To complete the comparison, Fig. 4 shows the increase in methane conversion beyond the equilibrium value obtained in the membrane reactor for all the catalysts. Note that the methane conversion almost doubles its equilibrium value at the highest sweep gas flow rates when the Rh/La–$SiO_2$ formulation is used.

### 3.2. Physicochemical characterization

#### 3.2.1. Supports

Table 2 shows the main characteristics of the supports. The diffractogram of the MgO shows the typical main reflections of the periclase structure at $2\theta = 43^\circ$ and $2\theta = 62^\circ$. After Ti grafting no crystalline titania is detected. However, new peaks appear in the diffractogram, which correspond to the formation of a new compound $Mg_2TiO_4$. The XPS data are consistent with the XRD findings for both the Mg 2s and the Ti $2p_{3/2}$ binding energies are different from those measured in the pure compounds (compare the B.E. data of the 2nd and 3rd row of Table 2). The textural properties of the MgO are not affected by the Ti grafting. Both are mesoporous solids (average pore diameter 25 nm) showing type II isotherms and type III hysteresis cycle in the high-pressure region.

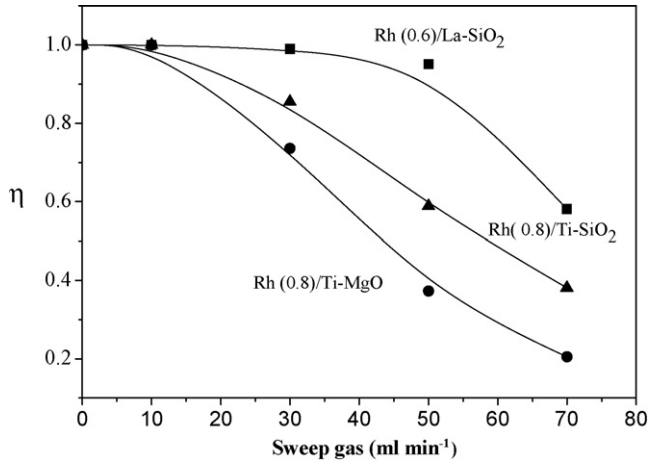


Fig. 3. Variation of the approach to equilibrium with increasing sweep gas flow rate $\eta = \prod_i p_i^{\nu i}/K_{eq}$. Conditions: same as Fig. 2.

After grafting Ti to silica, the new solid shows the characteristic diffraction lines of anatase crystallites with an average diameter of 19 nm. Two features of the XPS data call the attention: The increased value of the Ti $2p_{3/2}$ and the appearance of a second O 1s signal. They both reveal the presence of Ti–O–Si bonds in line with previous reports [9].

Two reflections appear in the La–$SiO_2$ that are absent in the starting amorphous silica. They are located at $2\theta = 29^\circ$ and $2\theta = 41^\circ$ and are assigned to $La_2Si_2O_7$ since these reflections coincide with the main peaks given for this compound (JCPDS No. 21-1014). In catalysts prepared by impregnating calcined silica with lanthanum nitrate, Vidal et al. [5] reported the formation of the same disilicate even for low lanthanum loadings.

#### 3.2.2. Fresh (F) and used (U) catalysts

Comparing the surface areas shown in Tables 1 and 2, there are no significant differences in surface areas between the catalysts and the support. Table 3 summarizes the main features of the catalysts. Concerning the information obtained from XRD, the only difference observed now (Tables 2 and 3) is the appearance of trace amounts of rhodium oxide and Rh$^\circ$ in the Ti–$SiO_2$ system. The laser Raman spectra of the three catalysts show the presence of graphitic carbon after use in the membrane reactor. The amount of carbon formed is, however, below the detection limit of our TGA instrument. As an example, Fig. 5 shows the triplet corresponding to the anatase in the low wave number region and the two characteristic graphite

Table 2
Physicochemical characterization of the supports

| Solid[a] | XRD | $S_{BET}$ ($m^2\ g^{-1}$) | XPS, B.E. (eV) | | | | |
|---|---|---|---|---|---|---|---|
| | | | Mg 2s | Ti $2p_{3/2}$ | Si 2p | La $3d_{5/2}$ | O 1s |
| MgO[b] | MgO periclase | 56 | 87.9 | – | – | – | 530.6 |
| Ti(7.0)–MgO | Periclase $Mg_2$–$TiO_4$ | 54 | 88.6 | 458.6[c] | – | – | 530.8 |
| $SiO_2$[c] | Amorphous | 94 | – | – | 104.0 | – | 532.7 |
| Ti(13)–$SiO_2$ | Anatase[d] | 98 | – | 459.2[c] | 103.4 | – | 532.7/530.4 |
| La(27)–$SiO_2$ | $La_2Si_2O_7$ | 150 | – | – | – | – | – |

[a] The weight percentage of $TiO_2$ and $La_2O_3$ are shown between brackets.
[b] Calcined 4 h at 973 K.
[c] For pure $TiO_2$ 458.2 eV.
[d] Anatase crystallites of 19 nm average diameter.

Table 3
Physicochemical characterization of the catalysts

| Catalyst | | XRD | LRS | TPR | | XPS B.E. (eV) |
|---|---|---|---|---|---|---|
| | | | | $T$ (K)[a] | $H_2$/Rh[b] | Rh $3d_{5/2}$ |
| Rh(0.8)/Ti–MgO | F | Periclase[c] $Mg_2TiO_4$[c] | | 678 | 1.52 | 309.5 |
| | U | Periclase[c] $Mg_2TiO_4$[c] | Graphite C | | | 306.6 |
| Rh(0.8)/Ti–$SiO_2$ | F | Anatase/$Rh_2O_3$[d] | Anatase | 436 | 1.56 | 308.8 |
| | U | Anatase/Rh°[e] | Graphite C | | | 307.0 |
| Rh(0.6)/La–$SiO_2$ | F | $La_2Si_2O_7$ | | 420 | 1.47 | 308.7 |
| | U | $La_2Si_2O_7$ | Graphite C | | | 307.6 |

[a] Maximum temperature of the $H_2$ consumption peak (See Fig. 6).
[b] $H_2$ consumed per Rh atom.
[c] Increased crystallinity compared to the support.
[d] Traces of rhodium oxide.
[e] Traces of Rh°.

signals located at 1340 $cm^{-1}$ and ca. 1590 $cm^{-1}$, observed in the used Rh/Ti–$SiO_2$ catalyst.

For comparison purposes, the TPR profiles shown in Fig. 6 include the data collected for Rh/$SiO_2$. Since it is well known that the metal/oxide interaction in the silica case is minimal, it is concluded that this technique indicates that the interaction of Rh with La–$SiO_2$ and Ti–$SiO_2$ are of similar strength while the bonding between the metal and the Ti–MgO is much stronger. In all cases, the $H_2$ consumption is essentially the same (Table 3) and corresponds to $Rh^{+3}$.

With the exception of Rh, the binding energies of all the other elements present in the three catalysts are not affected by exposure to the reacting atmosphere and therefore are not shown. The Rh binding energies of the fresh catalysts (Table 3) indicate that the prevalent species on the surface is $Rh^{+3}$. A more detailed analysis of the Rh 3d signal suggests the presence of small proportions of $Rh^{+}$ and even Rh° (<10%). After use, the Rh 3d bands move downwards clearly indicating that the element remains reduced (mainly Rh°) after reaction. The B.E. value of 306.6 eV measured for the used Rh-Ti–MgO catalyst is too low for metallic rhodium. At this point we have no explanation for this extremely low value that cannot be ascribed to a charge effect either.

Table 4 shows the surface concentration of the fresh and after use catalysts. Concerning Rh/Ti–MgO, the only effect observed after use is the sharp decrease of surface Ti atoms while the Rh exposure remains essentially constant. The explanation of this process might be found in the increased formation of the Mg–Ti compound which drives the surface titanium inside the MgO. On the Rh/Ti–$SiO_2$, the main effect is the decrease of the surface Rh. This might be explained by the sintering of Rh° (XRD shows the presence of the metal). Another option is the sublimation of Rh carbonyl during reaction. In the third case, the surface concentration of all the elements is not affected by the reaction atmosphere of the membrane reactor. Particularly, the constancy of the surface Rh concentration would indicate that the Rh dispersion remains constant after being on stream for 120 h.

## 4. Discussion

When Ti is grafted on MgO and La is impregnated on $SiO_2$, it can be observed that in both cases chemical reactions have occurred after calcination at 873 K. In the former, $Mg_2TiO_4$ was formed and in the latter, $La_2Si_2O_7$. The main reflection lines of these compounds are clearly seen in the diffractograms of these supports. A different interaction developed in the case of Ti–$SiO_2$. First of all, chemical bonds developed between the $SiO_2$ and Ti at surface level. The appearance of the second O 1s signal and the shift of the Ti $2p_{3/2}$ to higher B.E. (Table 2) are

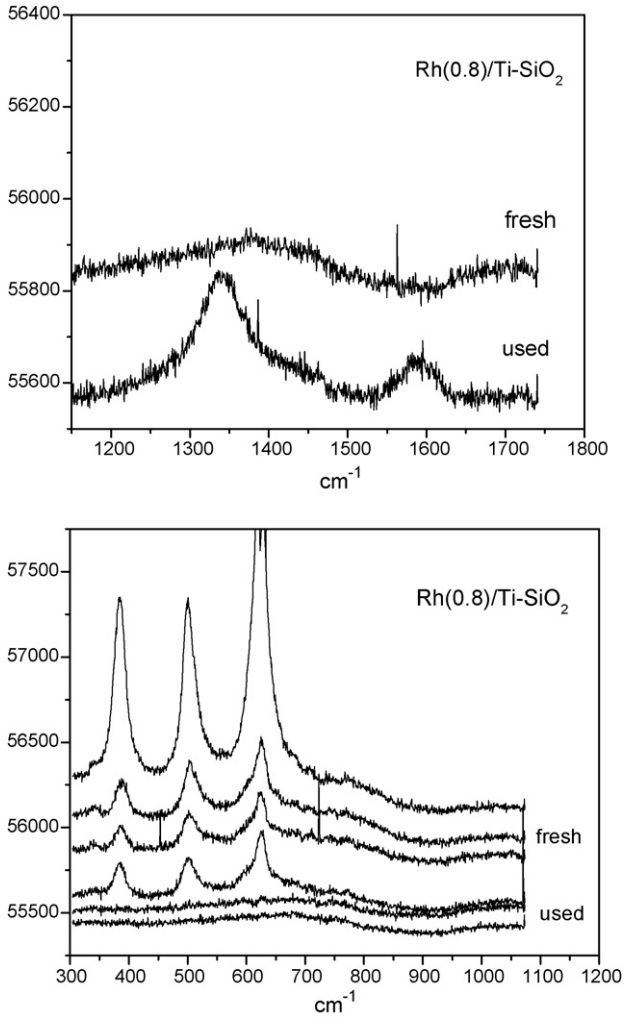


Fig. 5. Raman spectra of fresh Rh/Ti–$SiO_2$ and after use in the membrane reactor.

symptomatic of this interaction. On the other hand, the appearance of the main reflection of the anatase phase in the diffractogram of this support and the three bands seen in the Raman spectrum (Fig. 5) clearly indicate that a certain extent of heterogeneity develops in this case. The XPS data of the three supports are consistent with the XRD and Raman results.

When Rh is impregnated on these supports, different interactions are observed. The TPR profiles (Fig. 6) show that the Rh interactions decrease in the direction: Ti–MgO ≫ Ti–$SiO_2$ ≅ La–$SiO_2$. In the first case, it is known that $MgRh_2O_4$ is formed under certain conditions. Wang and Ruckenstein [10] impregnated 10% Rh on MgO and when they calcined the solid at 1173 K, the diffraction pattern of the mixed oxide became visible. The TPR profile of this solid showed two peaks at 623 and 803 K. In our case, with the solid treated at lower temperatures and fifteen times less Rh we cannot expect to see the XRD pattern of the mixed oxide. Nevertheless, the affinity between the two oxides may explain the strong interaction revealed by its TPR profile with a $H_2$ consumption peak at 678 K (Fig. 6). Besides, in our case the displacement of the Rh 3d signal to higher B.Es. (Table 3) might be symptomatic of the interaction of rhodium and the support.

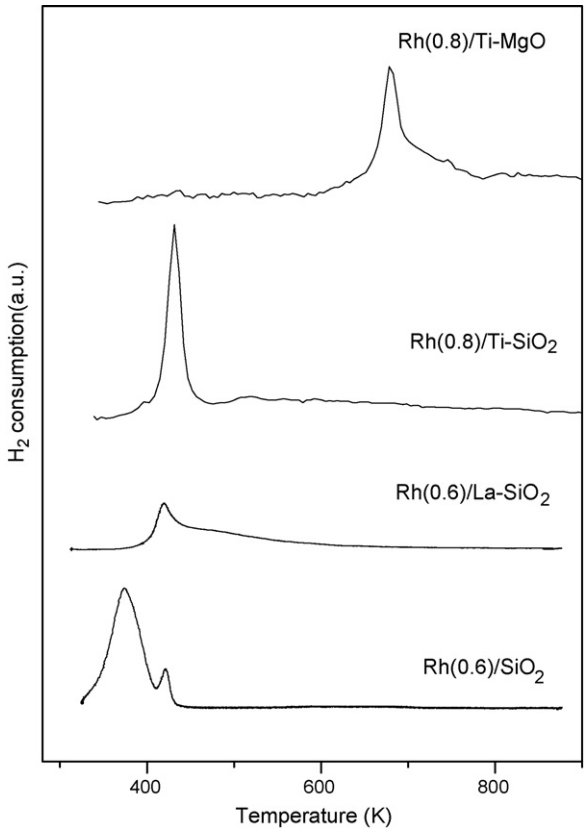


Fig. 6. Temperature-programmed reduction profiles ($H_2$(5%)/Ar, 10 K $min^{-1}$).

In the case of Ti–$SiO_2$, the partial segregation of $TiO_2$ revealed by both XRD and Raman techniques could explain the diminished metal/oxide interaction. Since at least part of the Rh could be grafted on the clean $SiO_2$ surface, it is not surprising that traces of $Rh_2O_3$ appear in the fresh solid, which are reduced to Rh° small crystallites in the used catalyst.

The La–$SiO_2$ contains lanthanum disilicate. The fact that no segregation of either rhodium oxides or metallic crystallites was revealed by XRD and the constancy of the Rh/(La + Si) surface ratio suggest that the high Rh dispersion on this support remains unaltered after use in the membrane reactor during 120 h.

The physicochemical description of the catalysts given above is completely consistent with the catalytic behavior of

Table 4
Surface atomic ratios of the fresh and used catalysts (membrane reactor)

| Catalyst | | Ti/Mg | Rh/Ti | Rh/Mg | Rh/Ti + Mg |
|---|---|---|---|---|---|
| Rh(0.8)/Ti–MgO | F | 0.21 | 0.08 | 0.02 | 0.016 |
| | U | 0.05 | 0.48 | 0.02 | 0.019 |
| Catalyst | | Ti/Si | Rh/Ti | Rh/Si | Rh/Ti + Si |
| Rh(0.8)/Ti–$SiO_2$ | F | 0.07 | 0.08 | 0.0052 | 0.0062 |
| | U | 0.06 | 0.13 | 0.0046 | 0.0044 |
| Catalyst | | La/Si | Rh/La | Rh/Si | Rh/La + Si |
| Rh(0.6)/La–$SiO_2$ | F | 0.04 | 0.1 | 0.0028 | 0.0027 |
| | U | 0.05 | 0.05 | 0.0028 | 0.0027 |

these rhodium-containing formulations in the membrane reactor. Thus, when the metal/oxide interaction is too strong (Rh/Ti–MgO), the lowest catalytic activity is observed. This is clearly seen in Fig. 3 that shows that this catalyst is not active enough to restore the chemical equilibrium when $H_2$ is being extracted from the reaction section of the membrane reactor. On the other extreme, Rh/La–$SiO_2$, the metal/oxide interaction is not so strong as in the previous case but stronger than on $SiO_2$. Again, Fig. 3 shows that this solid is able to restore the chemical equilibrium when an important $H_2$ permeation flux is forced in the membrane reactor. The Rh/Ti–$SiO_2$ shows an intermediate behavior as a result of the segregation of $TiO_2$ that makes the support heterogeneous. This is revealed by the appearance of traces of $Rh_2O_3$. This is possibly due to the interaction of Rh with uncovered $SiO_2$ surface.

## 5. Conclusions

- The three Rh-containing catalysts are active for the dry reforming of methane, stable for at least 120 h on stream, and only form traces of graphitic carbon detected by LRS but not measurable by TGA.
- The Rh/Ti–MgO shows the strongest Rh/oxide interaction and this may explain why this catalyst exhibits the lowest capacity to restore the $CO_2 + CH_4$ reaction equilibrium when $H_2$ permeates out of the reaction section of the membrane reactor (Fig. 3).
- The Rh/Ti–$SiO_2$ shows a lower Rh/oxide interaction and, due to the support heterogeneity, part of the Rh segregates to form traces of $Rh_2O_3$ (fresh solid) that evolve to $Rh^\circ$ crystallites in the used catalysts.
- The Rh/La–$SiO_2$ has a metal/oxide interaction similar to the previous system but due to the homogeneity of the support, no $Rh^\circ$ is detected after use. Furthermore, the Rh/(La + Si) ratio does not change by contact with the reacting stream and consequently it is unlikely that the metal dispersion has been affected.
- The methane conversion is well above the equilibrium value at 823 K for the three catalysts (Fig. 4) and particularly when Rh/La–$SiO_2$ was used, the methane conversion achieved at the highest sweep gas flow rate almost doubles the equilibrium conversion (50% vs. 26.4%).

In brief, a high, stable metal dispersion and an optimal anchorage of the Rh to the support seem to be key factors for high performance in the membrane reactor.

## Acknowledgements

The authors wish to acknowledge the financial support of the SECyT (Argentina)—FNRS (Belgium) program that allowed us to develop this collaborative effort. C.C., A.R., L.C. and EAL thank the UNL, CONICET and ANPCyT for the research grants that support their work. C.M.P. and P.R. thank the ‘‘Direction Générale des Technologies, de la Recherche et de l’Energie (DGTRE)’’ de la ‘‘Région Wallonne’’ (Bélgica) and the FNRS for financial support. Thanks are also given to Prof. Elsa Grimaldi for the edition of the English.

## References

[1] J. Múnera, S. Irusta, L. Cornaglia, E. Lombardo, Appl. Catal. A: Gen. 245 (2003) 383.
[2] S. Irusta, J. Múnera, C. Carrara, E.A. Lombardo, L. Cornaglia, Appl. Catal. A: Gen. 287 (2005) 147.
[3] L.M. Cornaglia, J. Múnera, S. Irusta, E.A. Lombardo, Appl. Catal. A: Gen. 263 (2004) 91.
[4] C. Mateos-Pedrero, C. Cellier, P. Ruiz, Catal. Today 117 (2006) 362.
[5] H. Vidal, S. Bernal, R. Baker, D. Finol, J. Rodríguez-Izquierdo, Appl. Catal. 208 (2001) 111.
[6] D. Lee, P. Hacarlioglu, S. Ted Oyama, Top. Catal. 29 (2004) 45.
[7] E. Kikuchi, Y. Chen, Stud. Surf. Sci. Catal. 107 (1997) 547.
[8] T. Beutel, O. Alekseev, Y. Rydin, V. Likholobov, H. Knozinger, J. Catal. 169 (1997) 132.
[9] X. Gao, I.E. Wachs, Catal. Today 51 (1999) 233.
[10] H.Y. Wang, E. Ruckenstein, J. Catal. 186 (1999) 181.